



Numerical Method to Predict Slip Length in Turbulent Channel Flow

N. M. Nouri[†], M. R. Rastan and S. Sekhavat

*School of Mechanical Engineering, Mechanical Engineering, Applied Hydrodynamics Laboratory, Iran
University of Science and Technology, Narmak, Tehran, Iran*

[†]Corresponding Author Email: mnouri@iust.ac.ir

(Received February 10, 2014; accepted April 15, 2015)

ABSTRACT

In the present research work, we introduce a new method for estimating the slip length on superhydrophobic surfaces. Hence, a dynamic force is added to momentum equations and velocity boundary condition is rewritten in a new form. Laminar and turbulent channel flows are considered and two force functions are used with different profiles to investigate their effects on results. The turbulent channel flow is considered at $Re_\tau = 180$ and the Large Eddy Simulation (LES) method has been applied to analyze this flow. All results indicate that this method can predict the streamwise slip length with a good accuracy, which is comparable with the Navier's method. So, using this numerical solution and also measuring pressure drop and mass flow rate in the channel, slip length can be calculated. Consequently, the errors and difficulties of slip length measurements in typical methods such as AFM and μ PIV would be eliminated.

Keywords: Superhydrophobic, Slip length, Non-conservative force, Large eddy simulation.

1. INTRODUCTION

From an economic point of view, drag reduction has been an important topic in hydrodynamics problems. Reducing the fluid frictional drag means increasing the system efficiency and decreasing energy losses. So, many studies have been conducted over years on this issue and some solutions such as microbubbles injection (McCormick and Bhattacharyya 1973), adding polymers (Xueming *et al.* 2002), riblets (Bechert *et al.* 1997), active blowing, and suction (Kim 1999) have been developed.

Recent researches in material science have led to creation of superhydrophobic surfaces. Many experiments have shown that slip and noticeable drag reductions are observed in flow passing over these surfaces. Tretheway and Meinhart (2002) used micron particle image velocimetry (μ PIV) to measure the velocity profile in a hydrophobic microchannel. They reported that the velocity slip reached approximately 10% of free stream velocity. Hao *et al.* (2009) used the same coating on their hydrophobic surfaces and achieved 10% to 30% pressure drop in smooth and patterned microchannel. They also used μ PIV and measured apparent slip velocity of about 8% of centerline velocity at the wall.

The hydrophobicity of the surface is specified by slip length, which is also an indicator of drag

reduction. Many researchers confirmed that higher slip length improves drag reduction. However, greater slip length is caused by a combination of surface chemistry and micro scale surface roughness. In many smooth hydrophobic surfaces, no drag reduction is observed, whereas in ultra hydrophobic surface with their very rough surface, pressure drop of up to 40% is reported (Perot and Rothstein 2004). Although this roughness is favorable in drag reduction, it changes to a controversial issue in hydrophobic surfaces, due to making uncertainties in wall position and therefore in slip length. For example, Choi *et al.* (2003) reported slip velocity over the hydrophilic surface due to the sensitivity of the analysis to channel height. Bouzigues *et al.* (2008) used three techniques for measuring slip length and they indicated that errors were linked to the method of determination of the wall location. To sum up, although the instrumentation in micro fluidic devices is vastly expanded, measuring the slip length has remained a challenge due to the fact that the scale must be addressed within a range of a few to hundreds of nanometer.

Besides, most numerical investigations have used a Navier's law to model super hydrophobic surfaces. Based on Navier's theory, the relationship that defines the slip length (b) is

$$u_0 = b \left. \frac{\partial u}{\partial y} \right|_w \quad (1)$$

Where u_0 is magnitude of the slip velocity at the wall and $\left. \frac{\partial u}{\partial y} \right|_w$ is the wall shear rate. Despite many researches indicating that slip length is linked to shear rate (Choi *et al.* 2003), it is assumed independent in numerical simulations, which is acceptable for moderate shear rates (Min and Kim 2004; Nouri *et al.* 2012). The most researchers used direct numerical simulation (DNS) or large eddy simulation (LES) to investigate the effects of hydrophobicity on drag reduction. You and Moin (2007) applied DNS and LES to analyze the flows around the circular cylinder with hydrophobic boundary condition at Reynolds numbers of 300 and 3900. At both Reynolds numbers, decreased drag is observed. Min and Kim (2004) used Navier’s slip model with DNS method to investigate turbulent channel flow of $Re_\tau = 180$ with hydrophobic walls. They assumed slip boundary condition in streamwise and spanwise direction and concluded that only the streamwise slip velocity led to the reduction in pressure drop. Nouri *et al.* (2012) performed a variety of slip lengths with Navier’s slip boundary condition in LES method and confirmed that a noticeable effect on the near wall turbulence structures occurred when the slip length was greater than a certain value.

As cleared in the literature, the slip length is one of the most important parameters in hydrophobic surfaces and drag reduction still remains an unresolved problem both in experimental and numerical investigations. And therefore, measuring slip length in experimental research works or estimating slip velocity in numerical works remains a challenging subject.

It is obvious that estimating the slip length without doing expensive experiments or using micro/nano instruments can be valuable. Knowing this parameter can help calculating slip velocity and drag reduction.

This paper is aimed to introduce a new method for estimating slip length in superhydrophobic surfaces. For this purpose, slip velocity at the wall is related to pressure drop, shear stress and the non-conservative force, which is added to momentum equations. It means that the no slip boundary condition only occurs when this added force is in the same order as wall shear rate, otherwise, the flow can slip on the wall, as it occurs on hydrophobic surfaces.

To investigate the flow behavior in numerical methods, some researchers have applied a force in streamwise direction. Xu *et al.* (2007) used the controlling force for a sustained reduction in the skin friction. Mamori and Fukagata (2011) performed a sinusoidal profile of the wall-normal body force in a fully developed turbulent channel flow to investigate skin-friction drag reduction effect of traveling wave-like as the wall-normal Lorenz force. Nouri *et al.* (2013) used non-

conservative force to model the effects of microbubbles on pressure drop in turbulent channel flow. However, adding the force to the momentum equations is not limited to these applications. Volavy *et al.* (2010) introduced a method to generate turbulence on the inlet of the channel for LES method by performing the force in particular points of the computational domain.

As mentioned before, in this paper a non-conservative dynamic force acts to oppose the flow. Also, each time, the slip velocity on the wall is corrected by a renewed boundary condition, which is related to added force and pressure drop. The simulation is performed in laminar and turbulent channel flow due to homogeneity in streamwise and spanwise directions. By this simulation, estimating slip velocity requires knowing pressure drop and mass flow rate. It should be noticed that to simulate the effects of hydrophobicity in this method, the slip velocity is obtained directly from boundary condition rather than using Navier’s model, which has been used by most researchers. In the next step, the slip length could be calculated by Navier’s law. In other words, most researchers calculate slip velocity and drag reduction of hydrophobic surfaces using slip lengths measured in experiment and utilized in Navier’s theory. But this inverse method can predict slip velocity by entering measured mass flow rate and pressure drop magnitudes in numerical simulation. Afterwards, calculated slip velocity and wall shear stress in simulation are placed in Navier’s theory. As a result, the slip length could be extracted.

From the practical point of view, this method not only overcomes the difficulties of measurement of slip length in experimental research works, but also it has the ability of investigating the effects of hydrophobic surfaces with slip boundary condition without having a certain slip length and also presents a new application of body force in momentum equations.

2. MATHEMATICS AND GOVERNING EQUATIONS

2.1. LES Equations

The Navier-Stokes and continuity equations for incompressible flows are

$$\frac{\partial u_i}{\partial x_i} = 0 \quad (2)$$

$$\frac{\partial u_i}{\partial t} + u_j \frac{\partial u_i}{\partial x_j} = -\frac{1}{\rho} \frac{\partial p}{\partial x_i} + \nu \frac{\partial^2 u_i}{\partial x_j \partial x_j} \quad (3)$$

LES is a three-dimensional unsteady methodology; with which the large-scale fluctuations are directly computed from the spatially filtered Navier-Stokes equations and the effect of small-scale fluctuations are modeled using the Sub-Grid-Scale (SGS) model.

The equations for LES are given by applying the filtering operation (denoted by the over-bar) to mass conservation and momentum equation

$$\frac{\partial \bar{u}_i}{\partial x_i} = 0 \quad (4)$$

$$\begin{aligned} \frac{\partial \bar{u}_i}{\partial t} + \frac{\partial}{\partial x_j} (\bar{u}_i \bar{u}_j) = & -\frac{1}{\rho} \frac{\partial \bar{p}}{\partial x_i} \\ + \nu \frac{\partial^2 \bar{u}_i}{\partial x_j \partial x_j} + \frac{\partial \tau_{ij}}{\partial x_j} \end{aligned} \quad (5)$$

where \bar{u}_i is the resolved velocity component in the x_i direction, and the \bar{p} , ρ and ν are the pressure, density, and kinematic viscosity, respectively. In the context of LES, τ_{ij} is called the SGS Reynolds stress, which is modeled and written as

$$\tau_{ij} = \bar{u_i u_j} - \overline{u_i u_j} \quad (6)$$

Substituting $\bar{u}_i = u_i - u'_i$ into Eq. (6), we obtain

$$\begin{aligned} \tau_{ij} = \bar{u_i u_j} - \overline{u_i u_j} - (\overline{u_i u'_j} - \overline{u'_j u_i}) - \overline{u'_i u'_j} \\ = L_{ij} + C_{ij} + R_{ij} \end{aligned} \quad (7)$$

Here $L_{ij} = \bar{u_i u_j} - \overline{u_i u_j}$ is a convection of large eddies driven by themselves, $C_{ij} = -(\overline{u_i u'_j} - \overline{u'_j u_i})$ is the interaction of large-scale and SGS components, and $R_{ij} = -\overline{u'_i u'_j}$ is the SGS describing the extraction of energy by small eddies.

These terms represent the ‘‘closure problem’’ as it relates to LES and requires to be modeled. Two widely used models are the Smagorinsky model (Smagorinsky 1963) and the dynamic Smagorinsky model (Germano *et al.* 1991). The current work applies the dynamic Smagorinsky model, which compensates for some Smagorinsky’s shortcomings. In the Smagorinsky model, the SGS stress tensor τ_{ij} is modeled by an eddy-viscosity concept:

$$\begin{aligned} \tau_{ij} - \frac{1}{3} \delta_{ij} \tau_{kk} = 2\nu_t \bar{S}_{ij}, \quad \bar{S}_{ij} = \frac{1}{2} \left(\frac{\partial \bar{u}_i}{\partial x_j} + \frac{\partial \bar{u}_j}{\partial x_i} \right), \\ \nu_t = c_s^2 \Delta^2 |\bar{S}|, \quad |\bar{S}| = \sqrt{2 \bar{S}_{ij} \bar{S}_{ij}} \end{aligned} \quad (8)$$

where ν_t is the eddy viscosity, \bar{S}_{ij} is a strain rate of the large-scale or resolved field, and $|\bar{S}|$ is its magnitude. In this model, the parameter c_s is called the Smagorinsky coefficient, which needs to be specified. In simulations, c_s is based on predetermined expressions that relate c_s to flow parameters, such as the Kolmogorov constant.

The main advantage of using the dynamic Smagorinsky model is that there is no need for artificial adjustments of SGS viscosity, such as damping function. For this purpose, two different filters are used: a grid filter and a test filter, which is twice the width of the first filter. By applying the test filter to the Navier- Stokes equations, we have

$$T_{ij} = \overline{\overline{u_i u_j}} - \overline{u_i u_j} \quad (9)$$

The resolved stress tensor is

$$L_{ij} = \overline{\overline{u_i u_j}} - \overline{u_i u_j} = T_{ij} - \hat{\tau}_{ij} \quad (10)$$

By replacing T_{ij} and $\hat{\tau}_{ij}$ with their respective prediction from the Smagorinsky model, we obtain

$$L_{ij} - \frac{1}{3} \delta_{ij} L_{kk} = 2C M_{ij} \quad (11)$$

where $\hat{\Delta}$ is the width of the test filter ($\hat{\Delta} = 2\Delta$) and

$$M_{ij} = \left(\hat{\Delta}^2 \left| \hat{S} \right| \hat{S}_{ij} - \Delta^2 \left| \bar{S} \right| \bar{S}_{ij} \right) \quad (12)$$

One way for solving Eq. (11) for C is to minimize the square error average over all independent tensor components, as represented by Lilly (1992)

$$c = \frac{1}{2} \frac{L_{ij} M_{ij}}{M_{ij}^2} \quad (13)$$

2.2 Force Balance

Due to the simplicity of measuring pressure drop and mass flow rate of the channel, many researchers consider the channel flow as a suitable case to study hydrophobic parameters. The present work introduces a new method in computing slip length based on channel experimental data. For this purpose, pressure drop and mass flow rate are measured in experimental and then used in numerical method as the input data.

In the steady flow in a channel, force balance between pressure gradient and wall shear stress exists which is shown in Eq. (14):

$$\frac{du}{dy} \Big|_{y=0} = -\frac{1}{2\mu} \left[h \frac{dp}{dx} \right] \quad (14)$$

Where: dp/dx is the pressure gradient in channel, h is the channel height, $du/dy|_{y=0}$ is the velocity gradient on the wall and μ is the viscosity of fluid. Considering the above relation and knowing the pressure drop from experiments, one can achieve the wall shear stress and its force. Therefore, we should first simulate the shear stress on the wall by using the non-conservative force. So, the body force $\vec{F} = (\vec{F}_x, \vec{F}_y, \vec{F}_z)$ with specific function is generated each time and is added to the momentum equations. The function of this force should have its maximum near the wall and gradually decrease as it goes further from the wall. The appropriate

function, which is determined among several profiles, was exponential as described by the following function:

$$\bar{F}(x, y, z) = (|F| \cdot \exp(-\frac{y}{2\sigma}), 0, 0) \quad (15)$$

Where: y is the normal distance from the wall, σ is standard deviation indicating the influence domination of force and F shows the maximum magnitude of force distribution. By adding this force to momentum equations, we would have:

$$\frac{\partial \bar{u}}{\partial t} + (\bar{u} \cdot \nabla) \bar{u} = -\frac{1}{\rho} \nabla P + \nu \nabla^2 \bar{u} + \bar{F} \quad (16)$$

It should be noticed that the integral of body force (F_T) throughout the control volume is equal to wall force. So, according to the pressure drop, the integral of body force (F_T) is constant in the simulation. Eq. (17) shows its magnitude.

$$F_T = \int_V \rho F_0 \exp(-\frac{y}{2\sigma}) dv \quad (17)$$

As mentioned before, σ determines the region influenced by force. It is assumed that the wall force affects channel flow as long as half of channel height at most, so the quantity of σ is chosen depending on how the affected region from force is less than this height. Hence, F_0 will be calculated based on σ and wall force (F_T) and then F_0 and σ can be specified as input data.

By applying the body force in the opposite direction of flow, velocity gradient appears in the simulations. This velocity gradient supplies part of the wall force. This force, noted as F_s and shown in Eq. (18), appears because of balancing boundary condition performance. So, this new velocity boundary condition would introduce:

$$F_s = \mu A \frac{du}{dy} \Big|_{y=0} \quad (18)$$

By considering the fact that the purpose of this method is applying a specified force (F_T) to the domain equal to pressure drop effect, at each time step, F_s must be detracted from the total force (F_T). Consequently, remaining force, shown by F_V , must operate in momentum equation. F_V could be positive or negative that means it could be either in the same direction as the flow or in the opposite direction. The direction of this part depends on velocity gradient and indeed on the magnitude of F_s . Eq. (19) displays F_V and the relation between F_V , F_s and F_T as represented in Eq. (20).

$$F_V = \int_V \rho F_{t,x} \exp(-\frac{y}{2\sigma}) dv \quad (19)$$

$$F_V = F_T - F_s \quad (20)$$

As shown in Eqs. (17) and (19), the profiles of F_T and F_V have the same function. However, their coefficients are different. F_0 is the coefficient of total force distribution and $F_{t,x}$ is calculated at each time step by substituting Eqs. (17), (18) and (19) into Eq. (20). This unsteady coefficient ($F_{t,x}$) is given by Eq. (21). In order to simplify Eq. (21), " q " is introduced by Eq. (22).

$$F_{t,x} = F_0 - \left(\frac{\nu A}{q} \frac{du}{dy} \Big|_{y=0} \right) \quad (21)$$

$$q = \int_y \exp\left(\frac{-y}{2\sigma}\right) dy \quad (22)$$

Now we can introduce the new boundary condition for channel, which is called balancing boundary condition. In this boundary condition there is a balance between pressure gradient, shear stress on wall, and the non-conservative force, as shown in Eq. (23):

$$\frac{du}{dy} \Big|_{y=0} = -\frac{1}{2\mu} \left[h \frac{dp}{dx} - 2 \int F_V dy \right] \quad (23)$$

Now the velocity on the wall can be obtained from:

$$u_0 = u_1 + \frac{y_1}{2\mu} \left[h \frac{dp}{dx} - 2 \int F_V dy \right] \quad (24)$$

In the above relation, u_0 denotes the stream-wise slip velocity, u_1 indicates stream-wise velocity in wall-adjacent grid node. It should be noticed that the current form of velocity boundary condition includes the slip on stream-wise direction and applies no slip condition on two other directions.

Considering two points can be helpful; first, to obtain the correct slip velocity, dynamic non-conservative force and adaptive boundary condition of balancing must update each other through simulation process. Second, one should note the capability of method in simulating no slip condition. If experimental data for the uncoated channel is used, zero slip velocity would appear.

3. DESCRIPTION OF THE TEST CASE AND NUMERICAL METHOD

The model is validated as it is applied to two different cases. First, we choose the laminar channel flow, of which the experimental results of slip condition and analytical solutions are available and then the turbulent channel flow would be studied.

The $0.4 \times 0.0005 \text{ m}^2$ channel is chosen for laminar flow. The periodic boundary condition is applied on the span-wise (Z) direction and the balancing boundary condition is used on the upper and lower walls. The computer code uses finite volume method with the second order finite difference

scheme in sufficient number of collocated grids.

In the next step, the turbulent channel flow is chosen and the large eddy simulation is used as the solution method. So, the non-conservative body force is added to filtered Navier-Stokes equations:

$$\frac{\partial \bar{u}_i}{\partial t} + \frac{\partial}{\partial x_j} (\bar{u}_i \bar{u}_j) = -\frac{\partial \bar{p}}{\partial x_i} + \nu \frac{\partial}{\partial x_j} \left(\frac{\partial \bar{u}_i}{\partial x_j} + \frac{\partial \bar{u}_j}{\partial x_i} \right) - \frac{\partial \tau_{ij}}{\partial x_j} - \sum_{k=1}^{N_B} \bar{f}_i \quad (25)$$

Reynolds numbers based on the half-channel height and the friction velocity are $Re_\tau = 180$ and the initial condition is a flow field with 20% turbulence intensity with the mean flow velocity of 15.63m/s in the streamwise direction. The flow has been solved on a fine mesh with a $65 \times 65 \times 65$ grid, along the three axes of x , y and z .

In the turbulent flow, channel dimensions are $4\pi\delta \times 2\delta \times 4/3\pi\delta$ where δ is the half-channel height. A uniform mesh is employed in stream-wise ($\Delta x^+ = \Delta x u_\tau / \nu \approx 35$) and span-wise ($\Delta z^+ = \Delta z u_\tau / \nu \approx 12$) directions, whereas in the wall-normal direction a non-uniform mesh with the hyperbolic tangent function is used. So, the distance of the first mesh point off the wall is $y^+ = \Delta y u_\tau / \nu \approx 0.52$. The farthest distance to the mesh in the centerline of the channel is equal to 13.8.

Two functions with different F_0 and σ are used to investigate the effects of different force distributions and parameters on the results. One of the force functions is mentioned in Eq. (15) and the other, as used by Nouri *et al.* (2013) in modeling bubbles effect, is Gaussian type with the following function:

$$\vec{F}(x, y, z) = (|F| \cdot \exp(-\frac{y^2}{2\sigma^2}), 0, 0) \quad (26)$$

Two standard deviations of 1.7×10^{-3} , 1.7×10^{-4} are considered and in each case F_0 is calculated by knowing pressure gradient and mass flow rate. The results were normalized by the friction velocity at the no-slip wall $u_{\tau,0}$ and channel half height. The superscript (+) denotes the non-dimensionalized flow parameters.

Using the open source Computational Fluid Dynamics (CFD) code, called the OPENFOAM, the filtered equations are solved. This computer code uses the finite volume method and it has been extensively validated for the LES method. To eliminate the pressure-velocity coupling, the PISO algorithm has been applied, the second-order central difference scheme is used for the diffusion and convection terms and the Crank-Nicholson scheme is applied for the time term discretization.

4. RESULTS AND DISCUSSION

4.1 Numerical Validation: Laminar Channel Flow

Before applying the force model to turbulent channel flow, we validated this model in laminar channel flow. The results are illustrated in Fig. 1. The mean velocities from analytical solution of two dimensional Poiseuille flow and force model show a good agreement. In this situation, nearly 20% of drag reduction is observed in both numerical and analytical solutions, which are in suitable agreement with experiment results of Nouri *et al.* (2012). They measured drag reduction of laminar flow in coated microchannel. The experimental detail can be found on technical report (Nouri *et al.* 2012) (unpublished).

Consequently, the validation and suitable accuracy of this model in laminar flow help us investigate ability of the method in predicting drag reduction and also the slip length in turbulent flow.

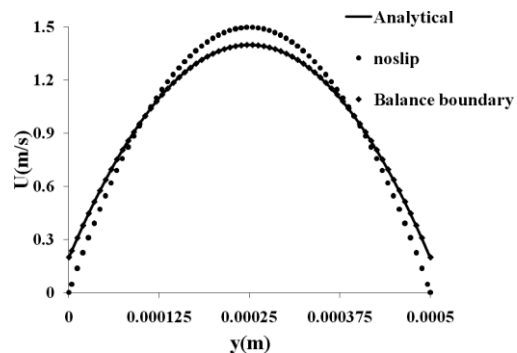


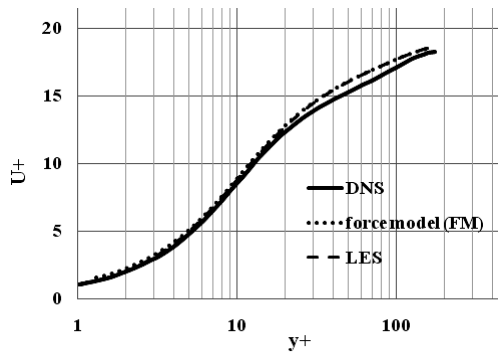
Fig. 1. Laminar channel flow with force model in slip condition.

4.2 Turbulent Channel Flow

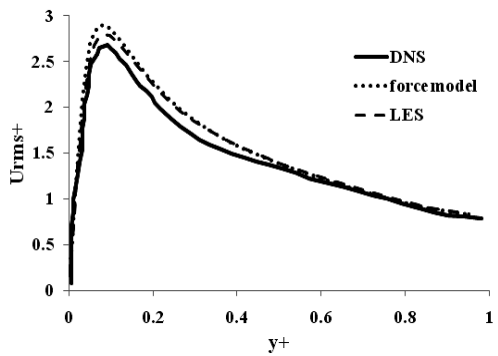
As the first step, the flow has been once solved with no slip condition using force model for two purposes, firstly to validate the numerical code again but this time in turbulent flow and secondly as the initial condition for solving the channel flow problem with the slip condition. So, the experimental data of the non-coated channel was used as input data for this part. Figure 2(a) illustrates a good agreement between mean velocities from DNS results (Min and Kim 2004), LES results (Nouri *et al.* 2012) and the current work. In Figs. 2(b), 2(c) and 2(d) root mean square of velocity fluctuations in the streamwise, wall-normal and spanwise directions are compared with those of DNS results for $Re_\tau = 180$. The results show acceptable accuracy in comparison with the DNS solution.

Reynolds stress is plotted in fig. 2(e). Reynolds stress is the magnitudes of the resolved shear and normal forces in the fluid and is assumed as the second-order turbulence characteristic. As expected, these results show acceptable accuracy in comparison with the DNS solution. These data are the valuable validation for the force model and the

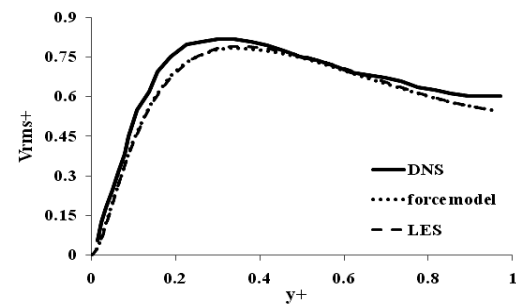
numerical code. So, the converged results of channel flow in this section were used as initial condition for solving the channel flow problem with the slip condition.



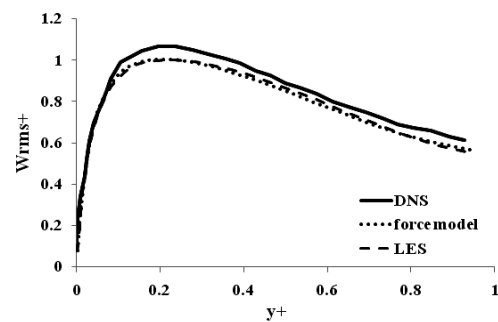
(a)



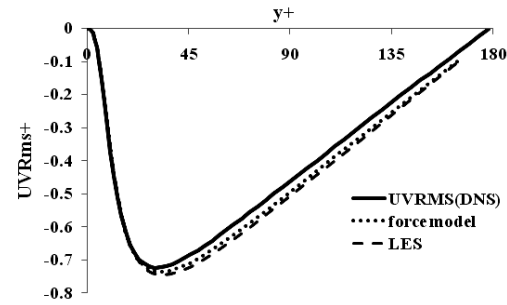
(b)



(c)



(d)



(e)

Fig. 2. Comparison of the current work, DNS (Min and Kim 2004) and LES (Nouri *et al.* 2012) (a) velocity profiles Root mean squares of (b) streamwise (c) wall normal (d) spanwise velocity fluctuations, (e) Reynolds stresses.

As mentioned earlier, to consider the effects of the force model in turbulent channel flow two force functions with different standard deviations are used. The results of the force function, which is presented by Eq. (15), have been shown in Fig. 3. Figure 3(a) illustrates the mean velocity profile for $\sigma = 1.7 \times 10^{-3}$ and different F_0 values, leading to various drag reductions. The root mean square of the velocity fluctuations in the streamwise, wall-normal, and spanwise directions are shown in Figs. 3(b), 3(c) and 3(d). Turbulence fluctuations are considered as part of the first-order turbulence nature and indicate the degree of turbulence intensity. As it shown in these figures, the turbulence fluctuations are severely reduced and increasing drag reduction weakens the near-wall turbulence structures. Reynolds stress is plotted in Fig. 3(e). This figure clearly depicts that the turbulence structures are affected by drag reduction and the Reynolds stress down-shifts even further by increasing the percentage of drag reduction. In these cases, the drag reduction can be calculated from the pressure loss in channel

$$DR = \frac{\left(-\frac{dp}{dx}\right) - \left(-\frac{dp}{dx}\right)_0}{-\frac{dp}{dx}\bigg|_0} \times 100 \quad (27)$$

It should be mentioned that for a constant σ different drag reductions are obtained by changing the initial value of F_0 , which can be calculated from different pressure drop values in experimental results.

To compare results of the present method with Navier's theory in slip condition, two different pressure-drop values and a specified mass flow rate, which lead to drag reductions of 9.22% and 28.26 are used as initial data. These magnitudes of drag reduction related in technical report of Nouri *et al.* (2012) (unpublished) and their corresponding pressure drop values can be calculated by Eq. (27).

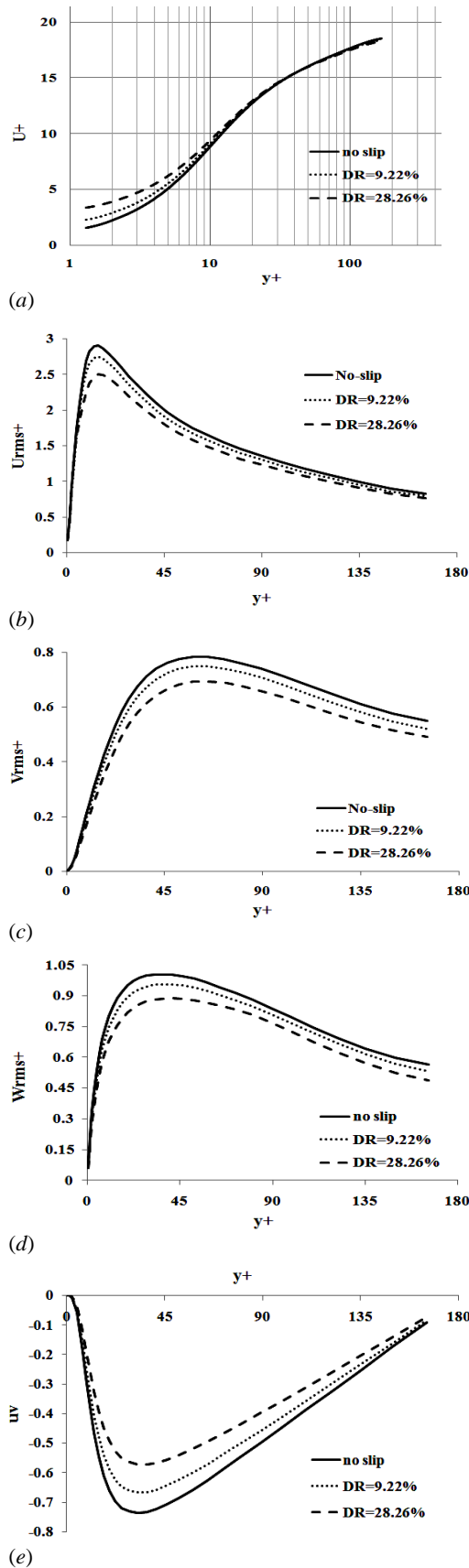
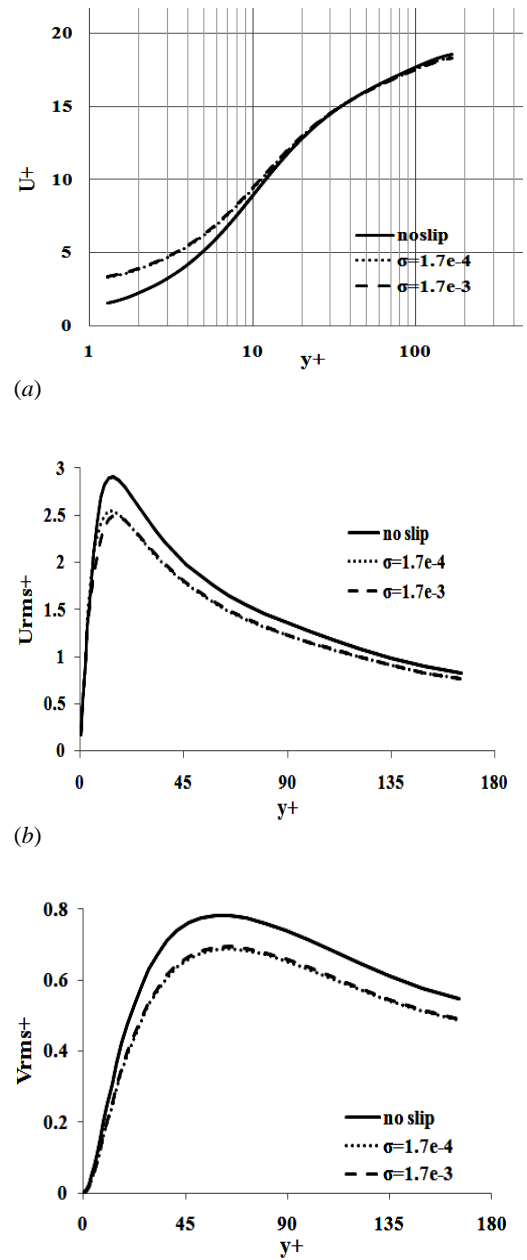


Fig. 3. (a) Mean velocity profile, Root mean squares of (b) stream-wise (c) wall normal (d) span-wise velocity fluctuations, (e) Reynolds stresses for force model with Eq. (15) and $\sigma = 1.7e-3$ in different drag reductions.

To analyze the effect of the standard deviation on results, we choose $\sigma = 1.7 \times 10^{-4}$ in the same force function. It is obvious that to get the same percentage of drag reduction, the initial value of F_0 must be changed and it would be greater than before. In other words, to achieve the same drag reduction or pressure drop, the volumetric integral of both force distributions must be the same. The mean velocity profile and velocity fluctuations are plotted in Figs. 4 (a-d). Reynolds stress is also shown in Fig. 4(e). These results are compared by previous results. As predicted previously, no remarkable change is observed by changing standard deviation.



(c)

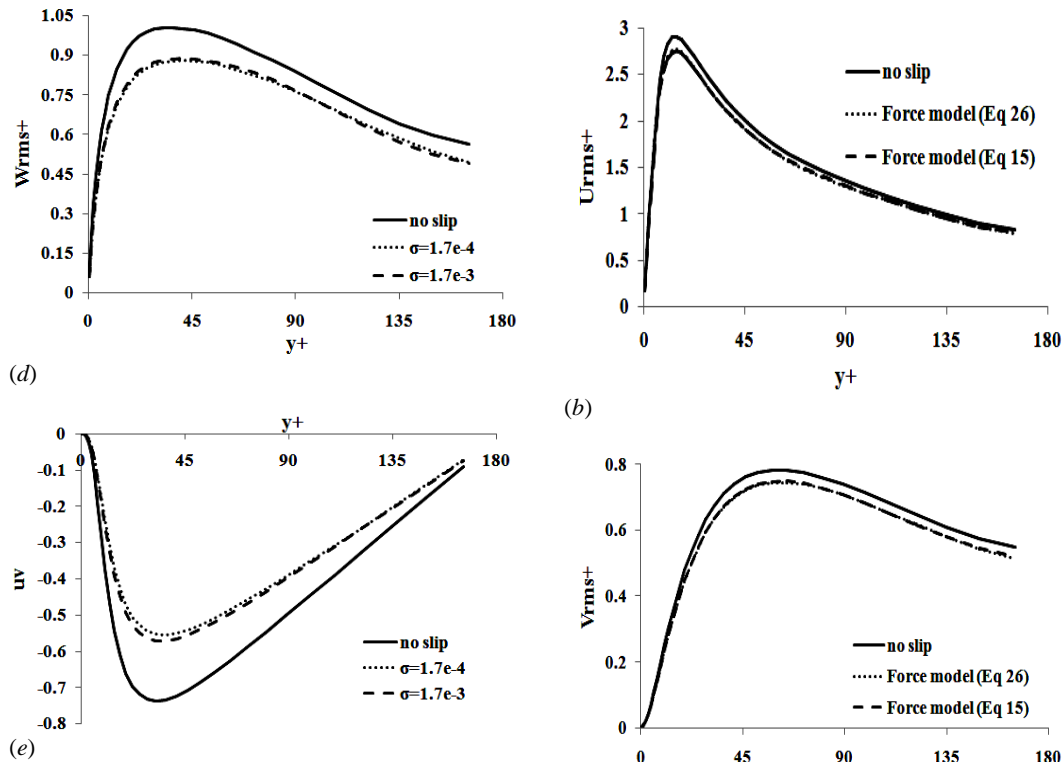
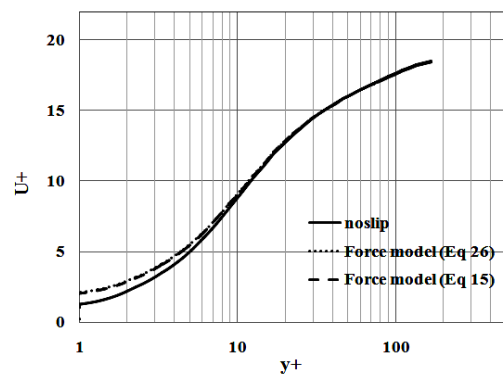


Fig. 4. Comparison of (a) mean velocity profiles, Root mean squares of (b) stream-wise (c) wall normal (d) span-wise velocity fluctuations, (e) Reynolds stresses for two different σ in DR=28.26%.

One of the most important issues in this research is to investigate the force function effect. Hence, the force function, indicated by Eq. (26), is considered. Figure 5 shows the results for two force functions at the same drag reduction. The standard deviations in these cases are the same. As indicated by these figures, the results remain close, which declares the insignificant effect of the force function on them. This conclusion is examined in other drag reduction values, as plotted in Fig. 6.

Table (1) shows the results from all cases and the comparison of Navier's theory at the same drag reduction. The results of Navier's theory are achieved by direct usage of Navier's hypothesis in LES method (Nouri *et al.* 2012).



(a)

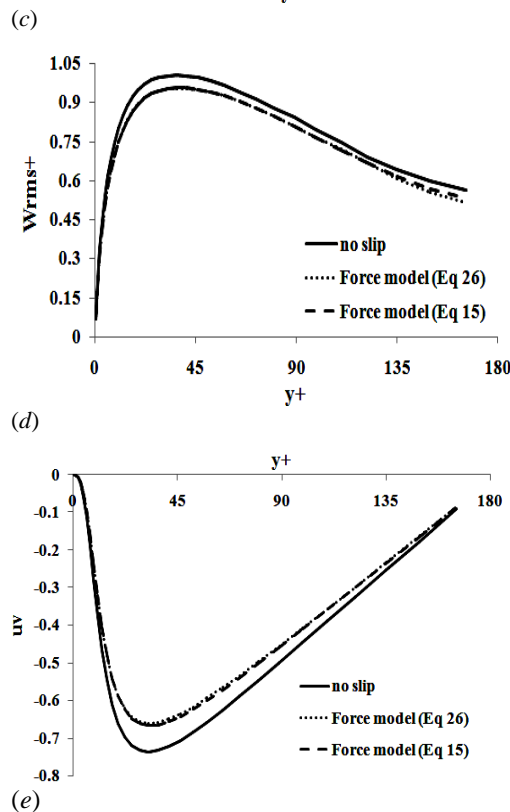
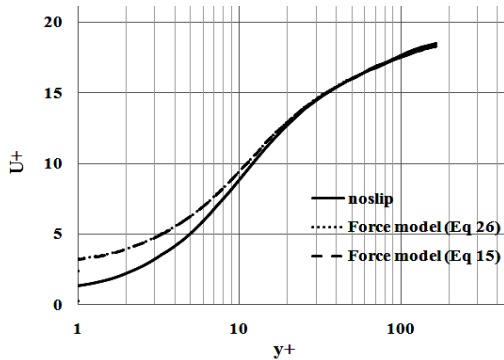
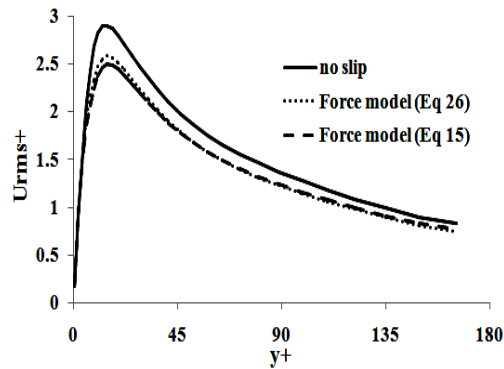


Fig. 5. Comparison of (a) mean velocity profiles, Root mean squares of (b) stream-wise (c) wall normal (d) span-wise velocity fluctuations, (e) Reynolds stresses for two force function in DR=9.22%.

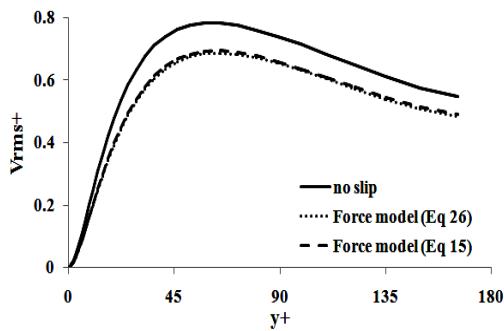
These results confirm that balancing boundary condition and force model are independent of force function and this model is capable of predicting the drag reduction and slip length without direct use of Navier's hypotheses in the simulation process.



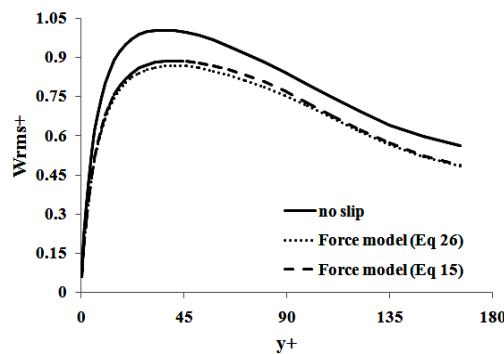
(a)



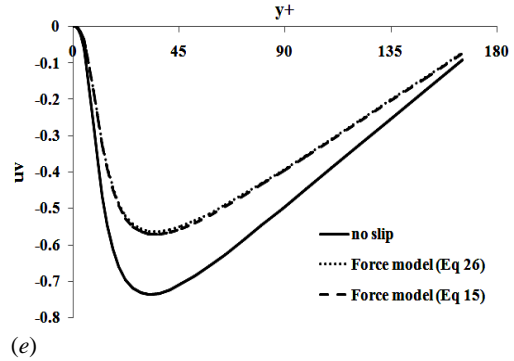
(b)



(c)



(d)



(e)

Fig. 6. Comparison of (a) mean velocity profiles, Root mean squares of (b) stream-wise (c) wall normal (d) span-wise velocity fluctuations, (e) Reynolds stresses for two force function in DR=28.26%.

5. CONCLUSION

Measuring the slip length of superhydrophobic surfaces is the most challenging part of estimating drag reduction. As researchers indicate, unrealistic slip length leads to different experimental and computational results.

This paper introduces a new method for predicting slip length on superhydrophobic surfaces. In this method, we only need pressure drop and mass flow rate, which is obtained from experiments and can be measured easily. These experimental data are set in the numerical solution in order to acquire slip velocity and velocity gradient on the wall. Finally, the slip length can be calculated from Navier's equation.

In this method, a body force is added to momentum equations and a new boundary condition, which is called balancing form update the velocity on the wall. This force is coupled to velocity boundary condition, and therefore, they modify each other within the solution. LES method is used for numerical simulation and two different force functions are applied in laminar and turbulent channel flows. The results are consistent with earlier researches, which are confirming that this method is capable of predicting the slip length. According to Table (1), 9.22% and 28.26% drag reductions are considered and the slip lengths with two force functions are obtained. Although the results of Gaussian distribution of force are closer to Navier's theory results, both cases show acceptable accuracy with this method. Furthermore, in all cases increasing the slip lengths leads to decreasing the shear stress and velocity fluctuations in the near-wall region. According to the previous DNS and LES researches on superhydrophobic surfaces, presented results confirm the ability of this new method in predicting flow behavior.

Consequently, using this method, slip length, which is one of the most important parameters in hydrophobic surfaces, can be achieved without using complicated and uncertain methods such as AFM and μ PIV.

Table 1 Slip length and drag reduction associated to force model in comparison with (Nouri *et al.* 2012)

	Force distribution	u_s	DR %	$L_s (m) \times 10^{-4}$	Navier's slip length (m) $\times 10^{-4}$
1	$F_0 \exp\left(\frac{-y}{2\sigma}\right)$	1.06	-9.32	0.584	0.5
2		2.29	-28.1	1.8	2
3		2.21	-27.9	1.74	2
4	$F_0 \exp\left(\frac{-y^2}{2\sigma^2}\right)$	1.09	-9.24	0.547	0.5
5		2.31	-28.34	1.89	2

ACKNOWLEDGEMENTS

The authors would like to appreciate Applied Hydrodynamics Laboratory of Mechanical Engineering School, Iran University of Science and Technology for facilities and fund for this work.

REFERENCES

- Bechert, D. W., M. Bruse, W. Hage, J. G. T. Vander Hoeven, and G. Hoppe (1997). Experiments on drag-reducing surfaces and their optimization with an adjustable geometry. *J. Fluids Mech.* 338, 59–87.
- Bouzigues, C. I., L. E. Bocquet, C. Charlaix, Cottin-Bizonne, B. Cross, L. Joly, A. Steinberger, C. Ybert and P. Tabeling (2008). Using surface force apparatus, diffusion and velocimetry to measure slip lengths. *Phil. Trans. R. Soc. A.* 366, 1455-1468.
- Chang-Hwan Choi, K. Johan A. Westin, and K. S. Breuer (2003). Apparent slip flows in hydrophilic and hydrophobic microchannels *Physics of Fluids* 15(10).
- Germano, M., U. Piomelli and P. Moin (1991). A dynamic subgrid scale eddy-viscosity model. *Physics of Fluids A* 3(7), 1760-1765.
- Hao, Peng-Fei, Wong, Catherine, Yao, Zhao-Hui and Zhu, Ke-Qin. (2009) Laminar Drag Reduction in Hydrophobic Microchannels. *Chem. Eng. Technol.* 32(6), 912–918.
- Kim, J. (1999). Active control of turbulent boundary layers for drag reduction. *Lect. Notes Phys.* 529,142–152.
- Lilly, D. K. and A. proposed (1992). modification of the Germano subgrid-scale closure method. *Physics of Fluids A* 4(3), 633-635.
- Mamori, H. and K. Fukagata (2011). Drag reduction by streamwise traveling wave-like Lorenz Force in channel flow. *J. Phys. Conf. Ser.* 318 022030. *Proc. 13th European Turbulence Conf. (ETC13), Warsaw, Sep 12-15, 2011, Paper 034, pp.*
- McCormick, M. E and R. Bhattacharyya (1973). Drag Reduction of a Submersible Hull by Electrolysis. *NAV ENG J.* 85, 11-16.
- Min, T. and J. Kim (2004). Effects of hydrophobic surface on skin-friction drag. *Physics of Fluids* 16, (7).
- Nouri, M. N, S. Sekhavat and A. Mofidi (2012). Drag reduction in a turbulent channel flow with hydrophobic wall. *Journal of hydrodynamics* 24(3), 458-466.
- Nouri, N. M., S. Yekani Motlagh, M. Navidbakhsh, M. Dalilbaghi and A. A. Moltani (2013). Bubble effect on pressure drop reduction in upward pipe flow, *Exp Therm Fluid Sci*, 44, 592–598
- Perot, J., B. Ou and J. P. Rothstein (2004). laminar drag reduction in microchannel using ultra hydrophobic surfaces. *Phys. Fluids.* 16, 4635-4643
- Smagorinsky J. (1963). General circulation experiments with the primitive equations: The basic experiment. *Monthly Weather Review* 91(3), 99-164.
- Tretheway, D. C. and C. D. Meinhart (2002). Apparent fluid slip at hydrophobic microchannel walls. *Phys. Fluid* 14, 9-12.
- Volavy, J., M. Forman and M. Jicha (2010). New Inlet Boundary Condition Treatment For Large Eddy Simulation *Colloquium. Fluid Dynamic*, Prague.
- XU, J., S. Dong, M. R. Maxey and G. E. Karniadakis (2007). Turbulent drag reduction by constant near-wall forcing. *J. Fluid Mech.* 582, 79–101.
- Xueming, S, L. Jianzhong, W. Tao and L. Yulin (2002). Experimental research on drag reduction by polymer additives in a turbulent pipe flow. *CAN J. Chem Eng.* 80, 293-298.
- You, D. and P. Moin (2007) Effects of hydrophobic surfaces on the drag and lift of a circular cylinder. *Physics of Fluids* 19, 081701.